J. Synchrotron Rad. (1999). **6**, 928–941

The identification of selected components in electron density maps of prokaryotic ribosomes at 7 Å resolution

Frank Schlünzen,[a] Ingo Kölln,[a] Daniela Janell,[a] Marco Glühmann,[a] Inna Levin,[b] Anat Bashan,[b] Jörg Harms,[a] Heike Bartels,[a,b] Tamar Auerbach,[b,c] Marta Pioletti,[d] Horacio Avila,[d] Kostas Anagnostopoulos,[d] Harly A. S. Hansen,[a] William S. Bennett,[a] Ilana Agmon,[b] Maggie Kessler,[b] Ante Tocilj,[a] Susanne Krumbholz,[a] Moshe Peretz,[b] Shulamith Weinstein,[b] Francois Franceschi[d] and Ada Yonath[a,b]*

[a]Max-Planck-Research Unit for Ribosomal Structures, Notkestrasse 85, 22603 Hamburg, Germany, [b]Department of Structural Biology, Weizmann Institute, 76100 Rehovot, Israel, [c]FU-Berlin, Department of Biochemistry and Pharmacology, Takustrasse 3, 14195 Berlin, Germany, and [d]Max-Planck Institute for Molecular Genetics, Ihnestrasse 73, 14195 Berlin, Germany. E-mail: csyonath@weizmann.weizmann.ac.il

(*Received 18 March 1999; accepted 11 May 1999*)

Crystals of small and large ribosomal subunits from thermophilic and halophilic bacteria, diffracting to 3 Å, are being subjected to structural analysis with synchrotron radiation. The bright beam necessary for detecting and collecting the diffraction at the higher-resolution shell causes significant decay even at 25 K. Nevertheless, data collected from native and heavy-atom-derivatized crystals led to the construction of electron density maps of both ribosomal subunits, showing recognizable morphologies and internal features similar to those observed by EM reconstructions of the corresponding ribosomal particle. The main features of these maps include elongated dense regions traceable as well separated RNA duplexes or single strands. Also seen are globular patches of lower density, readily distinguishable from the above, in which folds observed by NMR or crystallography in isolated ribosomal proteins at atomic resolution were detected. The intercomponents contacts identified so far reveal diverse modes of recognition. Metal clusters, attached at selected sites on the particles, are being exploited to facilitate unbiased map interpretation. In this way, two surface proteins were located and several surface RNA strands were targeted.

Keywords: ribosomes; complementary DNA; protein S11.

1. Introduction

The translation of the genetic code into polypeptide chains is performed on universal cellular organelles called ribosomes. These giant nucleoprotein assemblies (2.3 mDa in prokaryotes and 4.5 mDa in mammalians) are built of two independent subunits of unequal size that associate upon the initiation of protein biosynthesis. About one-third of the mass of prokaryotic ribosomes is comprised of up to 73 different proteins: the other two-thirds contain 4500 nucleotides arranged in three chains of ribosomal RNA (rRNA). Among these, 1500 nucleotides reside in the small ribosomal subunit and 3000 in the large one. Each of the two ribosomal subunits carries out different functional tasks. The large subunit (called 50S in prokaryotes) catalyzes the formation of the peptide bond and provides the path along which the nascent protein progresses. The small subunit (30S in prokaryotes) plays the major role in translation initiation, accomplishes the decoding of the genetic information and controls the translational fidelity.

Since ribosomes are composed of highly degradable RNA alongside with proteins which are often loosely held, and since they are prepared routinely as populations of a high conformational variability, they are difficult objects for crystallographic analysis. Therefore it was crucial to focus on relatively robust ribosomes from extremophiles. Maintaining crystal growth under conditions as similar as possible to the physiological environments, we obtained crystals of several ribosomal particles and their complexes (Table 1). Two of the crystal types grown by us diffract to 3 Å resolution (Fig. 1). These are of the large ribosomal subunits from *Haloarcula marismortui*, H50S (von Böhlen *et al.*, 1991) and of the small subunits from *Thermus thermophilus*, T30S (Yonath *et al.*, 1988; Harms *et al.*, 1999). The small ribosomal subunits are the particles exhibiting the lowest level of stability and the highest level of flexibility and heterogeneity (Berkovitch-Yellin *et al.*, 1992;

Gabashivili *et al.*, 1999). Interestingly, their crystals diffracting to the higher resolution were shown to contain particles with close to active conformation (Harms *et al.*, 1999).

The extremely weak diffraction power of all ribosomal crystals dictates absolute dependance on synchrotron radiation. For lower-resolution data collection, second-generation synchrotrons with insertion devices (*e.g.* BW6 or BW7 at DESY) were found sufficient but, for collecting quality data at the higher-resolution shells, above 5 Å, brighter synchrotron radiation is essential (*e.g.* F1 at CHESS, ID2 at ESRF, ID19 at APS). Unfortunately, the ribosomal crystals show severe radiation sensitivity even at He-stream temperatures (15–25 K) when using the bright synchrotron radiation beam required for high-resolution data collection. Thus, resolution decay (*e.g.* from 3 to 6 Å) is usually detected within a period sufficient for collecting a few frames, covering 1–1.5 degrees of rotation (Krumbholz *et al.*, 1998; Yonath *et al.*, 1998). Combined with the inherent low level of isomorphism of some types of ribosomal crystals, the rapid decay hampers efficient construction of complete data sets. To partially circumvent these problems we are using an X-ray beam with a cross section that is smaller than the longest axis of the crystals. Once decay is monitored by resolution loss, the crystals are translated, and a new section is irradiated (Fig. 1).

The generation of accurately measured signals from derivatized crystals at the higher-resolution shells was found to be a rather demanding task, mainly because of the enormous size of the ribosomes that cannot be subdivided by non-crystallographic symmetry. In addition, the problematic nature of the ribosomal crystals dictate not only careful data collection but also special attention in the assignment of phases. Even in cases of reasonable isomorphism, the identification of appropriate positions of heavy atoms for phasing is extremely time consuming, and each step in the course of phase assignment must be supported and validated by several methods or approaches. For these reasons the phasing is performed in a progressive fashion, from low to higher resolution.

Medium-resolution electron density maps of the small and the large ribosomal subunits were obtained recently using the isomorphous replacement method alone (Yonath & Franceschi, 1998; Yonath *et al.*, 1998; Harms *et al.*, 1999) or together with molecular replacement (Ban *et al.*, 1998). These contain the characteristic morphological features observed for the corresponding ribosomal particles by EM reconstructions that show their internal key features (Yonath *et al.*, 1987; Stark *et al.*, 1995; Frank *et al.*, 1995). Analysis of the features of the currently available maps should lead to interesting findings, and tracing attempts of the RNA chain, as well as assignment of protein domains, may be most illuminating. However, the accurate positioning of the ribosomal components poses additional challenges and requires additional structural information. The easier approach is to rely on the approximate identifications made within the EM reconstructions, exploiting

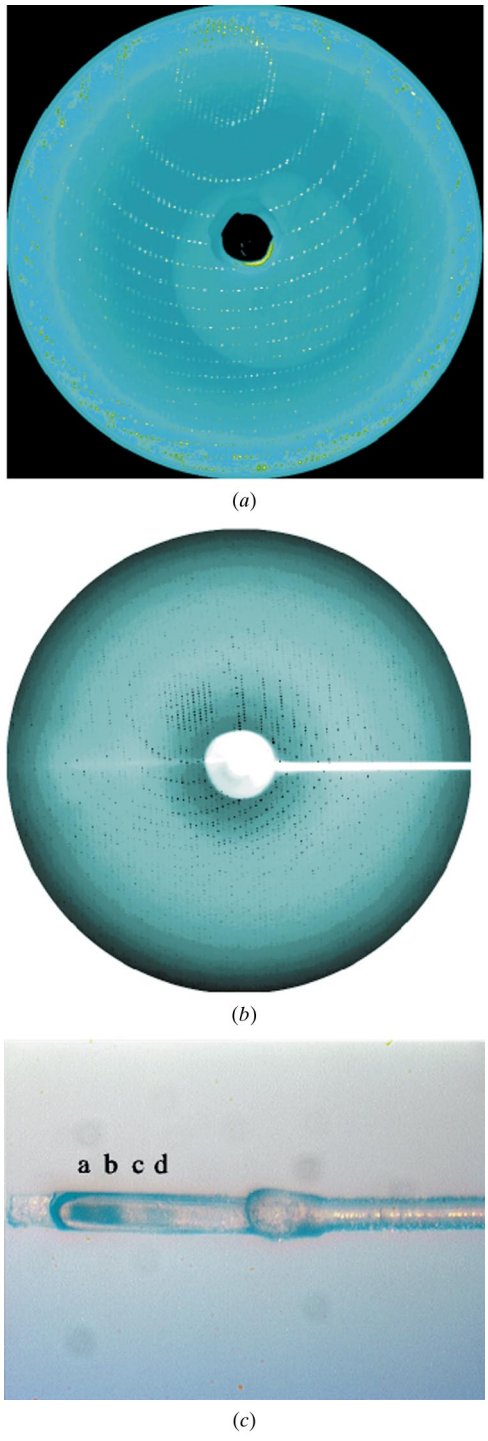

Figure 1
(*a*) Diffraction of 0.5° rotation obtained from a crystal of H50S soaked in 0.5 m*M* W30 (20" exposure) at ID13, ESRF. Resolution at the edge: 3.2 Å. (*b*) Diffraction of 0.5° rotation obtained from a T30S crystal at ID2, ESRF. Resolution at the edge: 3.5 Å. (*c*) A typical flat spatulum, with a mounted T30S crystal. The first position (marked *a*) was irradiated by a 65 µm beam at ID19, APS, and translated, once reaching 6 Å resolution (total 4°, 20 rotations. 0.2° each), to position *b*, where it was irradiated again. For clarity, position *c* was skipped, and at position *d* the crystal was exposed for only 15 s. Note that the intensities of the 'burns' are proportional to the exposure time. These burns were used to indicate which parts of the crystal had been exposed and damaged by the beam.

Table 1
Three-dimensional crystals of ribosomal particles used in this study.

Source	Grown form	Cell dimensions (Å)	Resolution (Å)
T70S	MPD†	524 × 524 × 306; $P4_12_12$	20–24
T70S‡	MPD	524 × 524 × 306; $P4_12_12$	14–17
T30S-LR	MPD	407 × 407 × 170; $P4_12_12$	10–12
T30S-HR	MPD	407 × 407 × 170; $P4_12_12$	3.0
T50S	AS†	495 × 495 × 196; $P4_12_12$	8.7
H50S	PEG†	211 × 300 × 567; $C222_1$	2.7

† MPD, AS, PEG = crystals grown by vapour diffusion in hanging drops from solutions containing methylpentanediol, ammonium sulfate or polyethylene glycol, respectively. ‡ A complex of T70S, two molecules phe-tRNA^{phe} and an oligomer of 35 uridines (as mRNA).

methods such as immuno-electron microscopy, neutron scattering with contrast variation, modelling based on crosslinking, footprinting, enzymatic activity and computational efforts, and to exploit this information for iterative phasing and map interpretation.

A more complicated and time-demanding approach, albeit more reliable and less biased, is being taken by us for independent assignments of the various ribosomal components. In this procedure, medium-size heavy-atom markers are attached at selected sites on the ribosomal surface either prior to or after crystallization. Despite the difficulties associated with their accurate localization in the electron density maps, we have so far elucidated possible sites of two specific cysteines and of several surface RNA strands (Weinstein *et al.*, 1999).

For both approaches, advantage may be taken of the structures of ribosomal components that have been determined (fully or partly) either by X-ray crystallography or by solution heteronuclear NMR. The uncertainties associated with the placements of structures determined for isolated ribosomal components into medium- or low-resolution maps of entire ribosomal particles should not be overlooked. These stem from the ambiguities which are likely to accompany fittings of frequently occurring structural motifs into medium-resolution maps, as well as from the possible conformational variability of the ribosomal components. An illuminating example concerns the attempts at fitting the coordinates of protein TL1 (Nikonov *et al.*, 1996). In one of these experiments a specific target within the 15 Å EM reconstruction of the large subunits from *E. coli* was chosen for the fitting, according to the suggestions resulting from immuno-electron microscopy (Malhotra *et al.*, 1998). In parallel studies, performed by us (Yonath & Franceschi, 1998), the entire 10 Å SIRAS map of the large subunit from *Thermus thermophilus*, T50S, the same source as that of protein TL1, was scanned for possible locations. This search led to positioning of protein L1 at various locations with similar scores, among them the position suggested by immuno-electron microscopy studies. Thus, it was clearly shown that, despite obtaining an apparent fit in the desired position, unambiguous positioning of ribosomal components requires supporting information as well as higher resolution. These studies also confirmed the observation that the structural motifs of protein L1 are rather popular among the ribosomal proteins (Liljas & Al-Karadaghi, 1997; Ramakrishnan & White, 1998). Interestingly, multiple assignment of common structural motifs occurred also when the 7.2 and 5.5 Å MIR maps of T30S were subjected to automated searches with no supporting information.

An additional source for uncertainties is connected to the long-lasting question: can the structures determined for individual ribosomal components represent the *in situ* conformation? Certainly the conformational variability of the isolated components is non-negligible and it is assumed that the *in-situ* conformations of the individual components may be influenced by their proximity to other r-proteins or rRNA. Protein S15 is an appropriate example, since the crystal structure of three-quarters of it was found almost identical to that determined by NMR, but significant deviations were observed for the remaining part (Clemons *et al.*, 1998). However, some relief concerning this open question may be gained from the cases in which the same crystal structure was determined for ribosomal proteins from different sources (Hosaka *et al.*, 1997; Wimberly *et al.*, 1997) or those showing that conformation variability is limited to the flexible part of the molecules (Clemons *et al.*, 1998; Draper & Reynaldo, 1999).

The main topics of this manuscript are the exploitation of a bright synchrotron radiation beam for higher-resolution ribosomal crystallography, and the resulting medium-resolution electron density maps of the large and the small ribosomal subunits. The maps obtained by us (Yonath *et al.*, 1998; Harms *et al.*, 1999) show various features, including elongated continuous dense features spanning the particles at various directions, traceable as single strands and double helices of rRNA, as well as globular or ellipsoidal regions of lower density, appropriate to accommodate ribosomal proteins. Inspection of the interactions between the ribosomal components revealed a diversity of modes of recognitions, in accord with observations made on smaller protein/RNA complexes (summarized by Cusack, 1999; Draper & Reynaldo, 1999). For the small subunit, the positioning of specific sites and the pinpointing of secondary structure elements of the ribosomal RNA are shown and several architectural elements are highlighted. However, as maps of higher resolution (*i.e.* 4–5 Å) are currently being constructed, with a quality that raises the expectations to reach the resolution limits, 3 Å, in the foreseeable future, extensive fitting has been deferred to later stages.

2. The current electron density maps

Careful alternations between clusters, organometallic compounds and heavy-metal salts (Table 2) combined with stepwise addition of phase information obtained by density modification procedures, led to 5–10 Å MIR, MIRAS and SIRAS maps of T30S, H50S and T50S, respectively. Deri-

vatization was performed by direct binding and by soaking. Ta_6Br_{14} (Harder & Preetz, 1990; Knäblein *et al.*, 1997) was found suitable for phasing the three crystal types, independent of the composition of the internal solvent of the crystal, namely MPD, PEG/KCl combinations or ammonium sulfate. For H50S, Ta_6Br_{14} yielded a prominent anomalous signal that was found stable up to 5 Å resolution (Weinstein *et al.*, 1999).

All three maps show shapes with overall appearance remarkably similar to the corresponding EM reconstructions, including recognizable internal features. All contain elongated continuous regions that span the particles at various directions, showing typical structure elements of RNA chains: single strands and double helices. The map of T30S also contains globular and ellipsoidal regions of lower density, appropriate for the accommodation of ribosomal

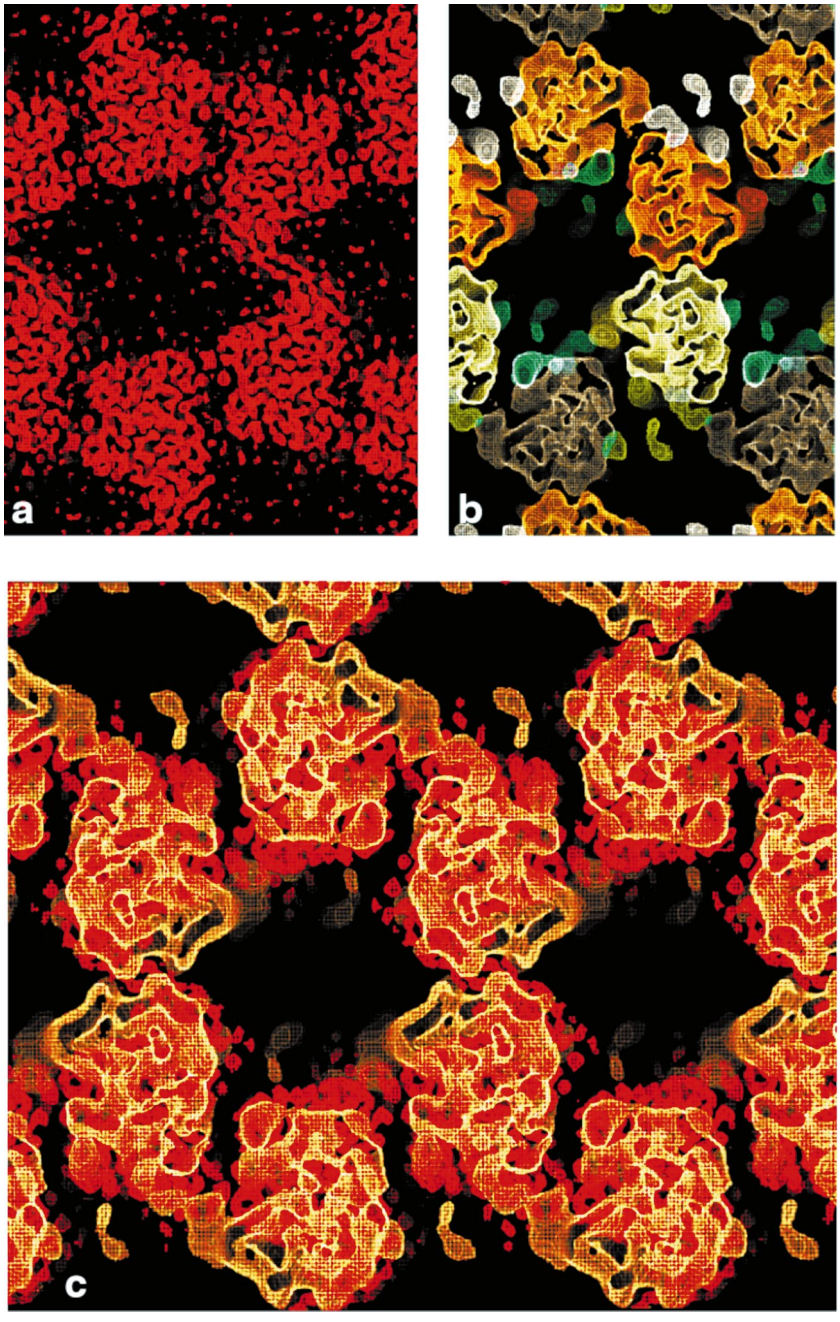

Figure 2
(*a*) A slab of about 25 Å of the MIRAS map of H50S (211 × 300 × 567 Å, $C222_1$), showing the packing arrangement of this crystal form: compact regions around z = 1/4 and 3/4 and a very small contact region at z = 1/2. For clarity, 1.5 cells are shown along the Y direction (horizontal). (*b*) A slab of about the same thickness made through the molecular replacement solution. For clarity, the main 50S particles are coloured yellow, gold, brown and beige. The smaller areas of density, coloured green, dark red and white, belong to the particles on top of or below the main ones. (*c*) The molecular replacement solution (in yellow) overlaid on the MIRAS map (in red), as shown in (*a*).

proteins. Because of the low contrast between average proteins and the internal solvent of H50S crystals, the protein regions are less well resolved in the 10 and 12 Å maps (Yonath *et al.*, 1998). However, at increased resolution the clarity of these regions is enhanced.

The solvent content of the ribosomal crystals studied by us falls within the range observed for other biomacromolecules (55–70%), but its distribution is rather unique. Thus, sizeable continuous solvent regions, with longest dimensions that may reach over 200 Å were detected in the inner part of all unit cells of H50S, T30S and T50S, regardless of the space group and the diffraction quality. In the unit cells of H50S (Fig. 2), each part bordering the solvent region is densely packed, but these densely packed regions are held loosely by one small interparticle contact area (Yonath *et al.*, 1998; Harms *et al.*, 1999).

For T30S, however, advantage could be taken of the bulky solvent region for improving the quality of the crystals. Assuming that the preferred conformation of the crystallized T30S particles is close to their active conformation, and that the solvent region is sufficiently large to allow for significant conformational rearrangements, the T30S-HR crystals were treated by controlled heating (Zamir *et al.*, 1971). Indeed, increasing proportions of crystals diffracting to 3–3.5 Å were obtained under conditions originally found to yield HR crystals of moderate resolution, *i.e.* 4.5–5 Å (Weinstein *et al.*, 1999).

3. The small ribosomal subunit

The small ribosomal subunit is the least stable among the ribosomal particles. For example, in attempts to crystallize functionally active 70S ribosomes, obtained by association of purified subunits, the 50S crystallized whereas the 30S subunits disintegrated into their individual components, and the 16S RNA became highly fragmented (Berkovitch-Yellin *et al.*, 1992). In another experiment when 70S ribosomes were exposed to a potent proteolytic mixture, the 50S subunits remained intact, whereas the 30S subunits were completely digested. High flexibility of the small subunit was also inferred from EM studies (Lata *et al.*, 1996; Harms *et al.*, 1999; Gabashivili *et al.*, 1999). Multiconformational states were suggested to account for the inconsistencies in locations of selected components revealed by surface probing (Alexander *et al.*, 1994) or by monitoring the ribosomal activity (Weller & Hill, 1992). Indeed, the early T30S crystals (Trakhanov *et al.*, 1989; Yonath *et al.*, 1988) yielded satisfactory data only to 10–12 Å resolution (Schluenzen *et al.*, 1995).

For over a decade these unfavourable properties could not be controlled. Recently, by optimizing the procedures for bacterial growth and employing milder conditions for ribosome purification and crystal treatment, we obtained diffraction to ∼3 Å from crystals of the small ribosomal subunits from *Thermus thermophilus* (called T30S-HR), that show tolerable isomorphism (Yonath *et al.*, 1998; Harms *et al.*, 1999). Employing the data-collection strategy mentioned above, complete data sets to 3.5–7.5 Å resolution were constructed from native and from derivatized crystals despite their high radiation sensitivity. Various heavy-atom compounds were used for soaking, ranging from the medium-size Ta_6Br_{14} and $C_2Hg_6N_2O_8$ to monometal compounds. Some of these were exploited for MIR and MIRAS phasing, leading typically to difference Patterson maps overcrowded with weak signals (Fig. 3). Over 50 sites originating from two relatively strong and two weaker derivatives that diffracted only to 7–7.5 Å were entered into the initial refinement procedure. This multisite binding led to reasonable phasing power, but imposed extensive cross-verifications. Performing step-by-step phasing, sufficient phasing power was obtained, allowing the construction of an interpretable MIR electron density map at 7.2 Å (Harms *et al.*, 1999; Weinstein *et al.*, 1999).

Table 2
Dense multimetal compounds used for these studies.

	Name	Formula
TAMM	Tetrakis(acetoxymercuri)-methane	
		Ta_6Cl_{14}
Hg6		$C_2Hg_6N_2O_8$
TIR	Tetrairidium cluster	$Ir_4(CO)_8R'_3R''$†
W17		$Cs_7[P_2W_{17}O_{61}Co(NC_5H_5)].14H_2O$
W12		$Na_{16}[(O_3PCH_2PO_3)_4W_{12}O_{36}].40H_2O$
W30		$K_{14}(NaP_5W_{30}O_{110}).31H_2O$

† Designed for covalent binding. R' = $P(CH_2CH_2CONH_2)_3$; R'' = $P(CH_2CH_2CONH_2)_2(CH_2CH_2CONHCH_2CH_2NH_2)$. The activation was *via* the primary amino group. [For references, see Wei *et al.* (1998) and Weinstein *et al.* (1999)].

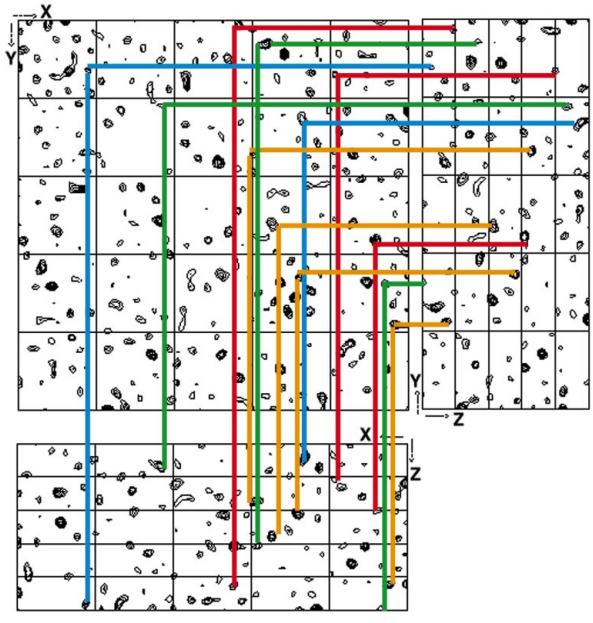

Figure 3
Three Harker sections of difference Pattersons maps of T30S constructed at 7 Å. Derivatization was performed with Ta_6Br_{14}. For clarity, not all possible sites were marked.

This map was partially extended to 5.5 Å by solvent-modification techniques. Since derivatives diffracting to 3.6–4 Å resolution were identified recently, the extension of the resolution of the current map, using experimental phases, is in progress.

3.1. *Main features of the 30S map*

Analysis of the 7.2 Å MIR map of T30S revealed recognizable features, resembling those seen in the EM reconstructed T30S particle at close to its active conformation, namely the part assigned to 30S within the reconstruction of the 70S ribosome. It shows the traditional division of the 30S subunit into three main parts (Stark *et al.*, 1995; Frank *et al.*, 1995; Lata *et al.*, 1996; Gabashivili *et al.*, 1999). These include a head, a rather narrow neck and a bulky lower body. Interestingly, the neck seen in the 7.2 Å MIR map is of a shape resembling that obtained at 23 Å by the three-dimensional EM reconstruction of E30S, published recently (Gabashivili *et al.*, 1999), whereas the side lobe (also called the platform) that originates from the body near the neck resembles that seen in the 24 Å reconstructions of T70S and T30S (Stark *et al.*, 1995; Harms *et al.*, 1999). Also seen are several finer details, among them those observed recently by cryo-EM of single particles. These include the groove that presumably facilitates the mRNA progression during the decoding process, located at the neck's level, and two smaller features, the beak, protruding from the head, and the toe (also called spur), extending from the lower part of the body, called the foot (Stark *et al.*, 1995; Frank *et al.*, 1995; Lata *et al.*, 1996; Gabashivili *et al.*, 1999).

The 30S head is known to be of a high inherent flexibility. The map shows that in the HR crystals the particle's heads are involved in interparticle contacts (Harms *et al.*, 1999). These may hinder their movement, thus acquiring stability, expressed in the high resolution of these crystals. Noteworthy is that in the 7.2 Å MIR map the heads show tertiary organization of rRNA double helices of remarkable similarity to that postulated in modelling attempts based on cryo-EM reconstruction and biochemical and cross-linking data (Mueller & Brimacombe, 1997). The head's involvement in the crystal network is part of prominent pairing around the crystallographic twofold axis (Fig. 4). Preliminary interpretation suggests that many of the pairing contacts are formed between the areas on the 30S surface which have high binding affinity. Primarily, however not exclusively, these contacts may mimic some of those formed between the small and the large subunits within the assembled ribosome.

As mentioned above, advantage was taken of the large internal solvent region, for the improvement of the quality of the crystals of T30S. This was achieved by performing functional activation of the ribosomal particles while in the crystals by controlled heating. Along these lines, improvement of crystal quality was also achieved when crystallizing T30S particles trapped chemically at their activation state prior to crystallization or complexed with antibiotics, such as edeine, that are known to 'freeze' the 30S subunits at a particular conformational state (Moazed & Noller, 1990).

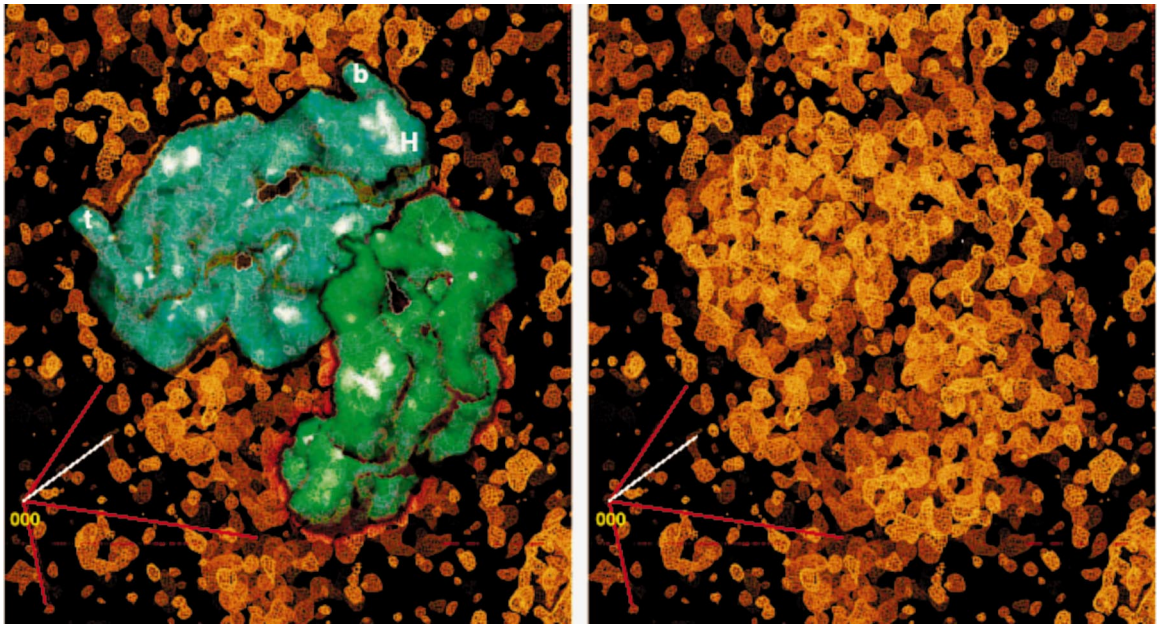

Figure 4
A pair of reconstructed T30S particles, painted blue and green, as extracted from the EM reconstruction of T70S by removing the part assigned as T50S, overlaid on a part of the 7.2 Å MIR map (shown on the right), featuring a pronounced 'toe' (t) at the foot of the 30S subunit and a significant-size beak (b) stemming from the head (H). The density seen between the two particles belongs to a lower particle. For comparison, the same part of the map is shown on the right. The directions of the unit-cell axes are shown in red, and that of the crystallographic twofold axis between the pair of T30S in white.

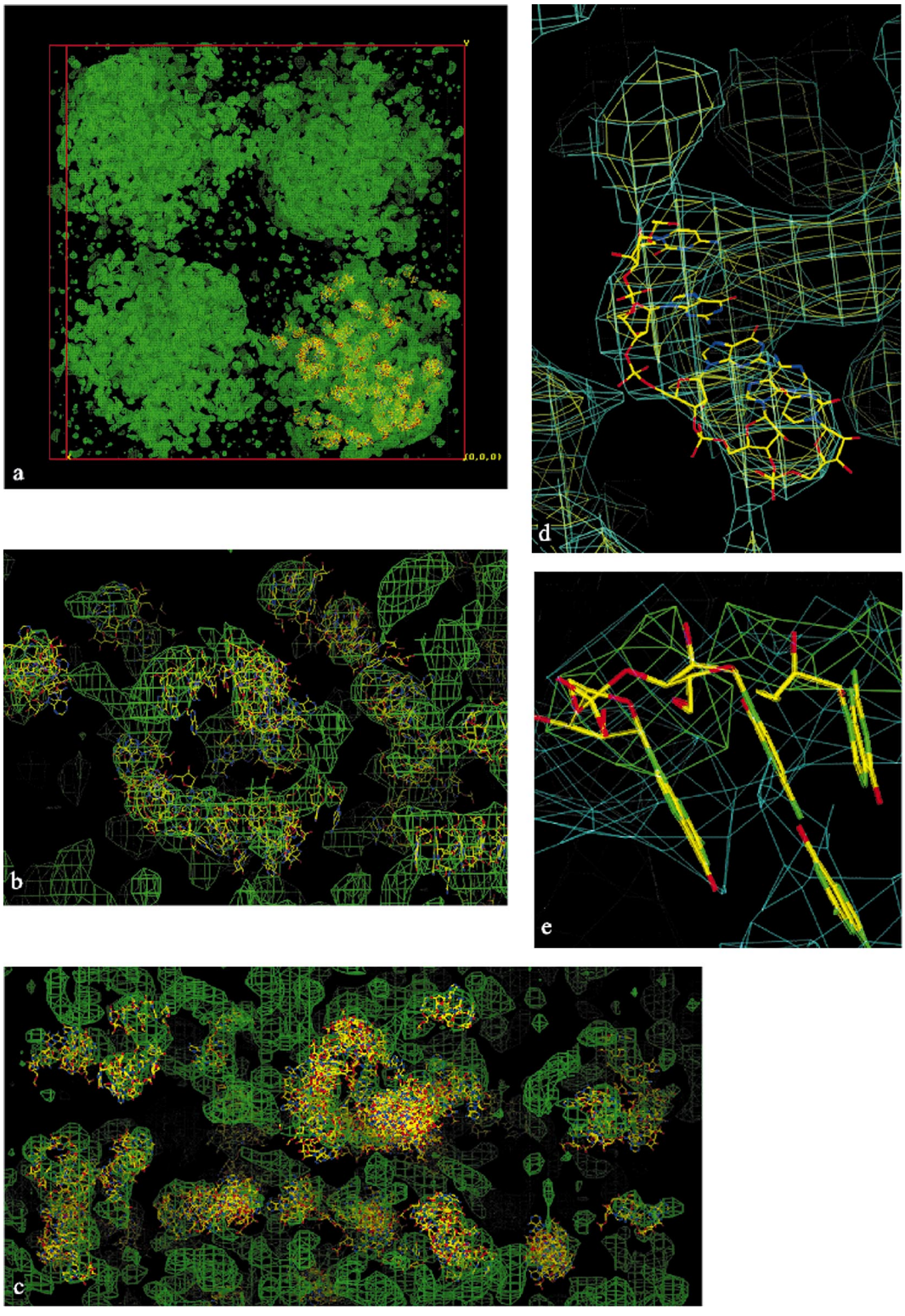

Figure 5
(*a*)–(*c*) RNA-rich regions, as detected by the program *ESSENS*. Groups of 6–22 nucleotides with commonly observed RNA folds (*e.g.* duplexes or single chains) were used. One T30S pair was subjected to the search and all the suggestions provided by the program for RNA assignments are shown. (*a*) The *Z* projection of the entire tetragonal unit cell. Note the apparent pairing in each corner around the twofold axis. Only a single T30S pair was subjected to the search. (*b*) and (*c*) Details from (*a*) showing the RNA regions along the interparticle contact area. (*d*) Part of the 7.2 Å MIR map of T30S that was manually assigned as a single-stranded RNA chain and a stretch of six nucleotides fitted into a part of it. Note the contacts made between this chain and its neighbouring regions. (*e*) A part of the 7.2 Å MIR map of T30S, manually fitted as a well separated RNA duplex. One base pair is clearly shown. Note the higher density (in green) along the main chain.

3.2. *Selected components and architectural elements*

The 7.2 Å MIR map of T30S reveals a wealth of internal features. The dense elongated chains that span the 30S particle at various directions show features similar to those detected in nucleosome core particles at comparable resolution (Richmond *et al.*, 1984). Some of these were manually traced either as separated RNA double helices or as single RNA strands (Fig. 5). In other cases the detection of regions crowded by the known motifs of rRNA or those frequently observed in ribosomal proteins was assisted by the program *ESSENS* (Kleywegt & Jones, 1997), although this program frequently suggested multiple solutions and did not always reveal the best assignments.

Continuous regions of lower average density of this map have been interpreted as specific motifs of ribosomal proteins, especially those suggested to interact with rRNA. Protein S7 was among the first proteins subjected to such a search. It was chosen owing to its biological importance and due to the high confidence in its crystal structure. Thus, two independent studies, performed on crystals of this protein from two bacterial sources, *Bacillus stearothermophilus* and *Thermus thermophilus*, led to essentially the same structure (Hosaka *et al.*, 1997; Wimberly *et al.*, 1997). Indeed, both the manual and the automatic searches suggested localization of this protein in approximately the same place, in reasonable agreement with the positioning of this protein within the borders of the EM reconstruction (Tanaka *et al.*, 1998). In this presumed position, the two residues of this protein that can be crosslinked with their neighbouring rRNA were found in close proximity to regions showing prominent high density, suitable to host rRNA (Fig. 6).

Hints for the provision of stabilization of the three-dimensional fold of the rRNA chains by ribosomal proteins were detected in several locations of the map. Two of them were tentatively assigned as proteins TS7 and TS4, in accord with the studies indicating that the 30S assembly is initiated by their binding (Novotny & Nierhaus, 1988). A different behaviour was observed for S15. In isolation, this protein is built of three well packed α-helical chains, and one helix which exhibits structural flexibility (Clemons *et al.*, 1998). In our trials to position this protein, a tentative location was suggested, in which most of the fold of this protein shows reasonable fit with the 7.2 Å MIR map, less density was found at the location where the flexible arm should be positioned if the crystallographic structure determined in isolation is maintained within the ribosome. In fact, neither the MIR 7.2 Å map nor its extension to 5.5 Å show clear indications for the location of this flexible arm (Fig. 7).

3.2.1. *Flags and markers.* As mentioned above, in order to facilitate unbiased map interpretation, flags and markers inserted in predetermined sites are being exploited. These are composed of heavy-atom compounds, attached either directly to the T30S particle or through carriers that bind to the ribosomal particles in specific sites with a high affinity. Examples are antibiotics, complementary DNA (cDNA) oligomers, charged tRNA molecules and factors participating in the translation process. Single heavy-atom and medium-size materials, such as TAMM and a tetrairidium cluster, TIR (Table 2), are used for this aim. The latter is composed of an internal core of four Ir atoms, with a diameter of 4.8 Å, surrounded by a shell of organic moieties of chemical composition similar to that of proteins (Jahn, 1989).

Labelling studies showed one fully and one partially exposed —SH group (Sagi *et al.*, 1995), belonging to proteins TS11 and TS13 (Wada *et al.*, 1998). These were used for cluster binding, prior to the crystallization. The crystals obtained from the so modified particles diffract to 4.5 Å resolution and are isomorphous with the native ones. As expected, the attachment of one to two equivalents of the tetrairidium cluster yielded a weak derivative, albeit a powerful marker. Thus, two prominent peaks were revealed in the electron density map using the amplitudes of the data collected from the TIR-modified crystals with the 7.2 Å MIR phases of T30 (Weinstein *et al.*, 1999).

The minor site, assigned as the TIR compound bound to the cysteine of TS13 (Wada *et al.*, 1998), is located on the particle's 'head' (Fig. 8) in a position similar to that of TS13, as determined for the *E. coli* 30S by immuno-electron microscopy (Stöffler & Stöffler-Meilicke, 1986), modelling (Mueller & Brimacombe, 1997) and neutron scattering (Capel *et al.*, 1988; Stöffler & Stöffler-Meilicke, 1986; Mueller & Brimacombe, 1997). The major site, assigned as the cys of TS11, is located at the central part of the particle, in a location roughly compatible with that suggested by immuno-electron microscopy for protein S11 in *E. coli* 30S (Stöffler & Stöffler-Meilicke, 1986), as well as that

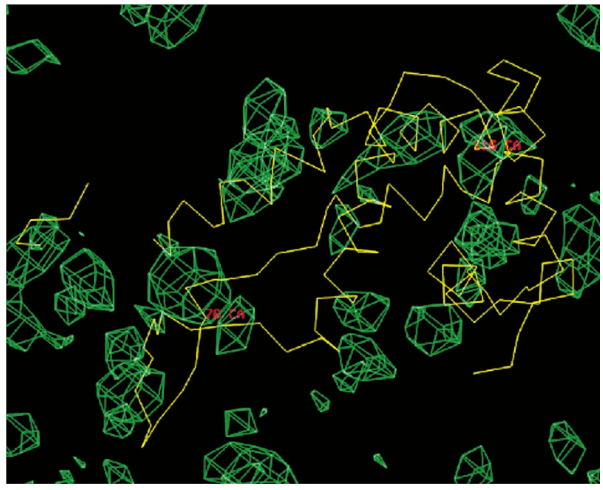

Figure 6
The backbone of proteins S7 positioned at its approximate location [as suggested by Mueller & Brimacombe (1997)] in an area showing many of its structural features and the highest density contours of the T30S 7.2 Å map in its vicinity. The map is contoured at 1.5σ, a level chosen for indicating the possible locations of RNA chains, while minimizing the visual interference with the protein location. Highlighted are the amino acids that were found closest to the RNA by crosslinking experiments (Tanaka *et al.*, 1998).

suggested by modelling the ribosomal components within cryo-EM reconstructions (Mueller & Brimacombe, 1997). However, it deviates by approximately 35 Å from the position assigned to the centre of mass of this protein by studies exploiting neutron scattering and contrast variation (Capel *et al.*, 1988). Since the tetrairidium cluster and immuno-electron microscopy target the surface of the ribosomal particles, whereas the triangulation method approximates the positions of the centres of mass of the ribosomal proteins, this deviation is tolerable. In fact, it is smaller than the inconsistencies of 65 Å between neutron-scattering triangulation studies and those exploiting complementary DNA for the localization of ribosomal components (Alexander *et al.*, 1994).

One of the limiting factors associated with these studies is the length and the flexibility of the bridging arm of the tetrairidium cluster. To minimize its flexibility we designed a bridging arm of minimal length and maximal stability. It is slightly longer than the longest amino acid side chain, and contains an amide bond (R'' in Table 2). Hence, the expectations for local rather rigid conformations are legitimate. Indeed, based on the resolution to which the TIR-modified crystals diffract, *i.e.* 4.5 Å, it seems that the crystallization of the modified T30S particles limited the

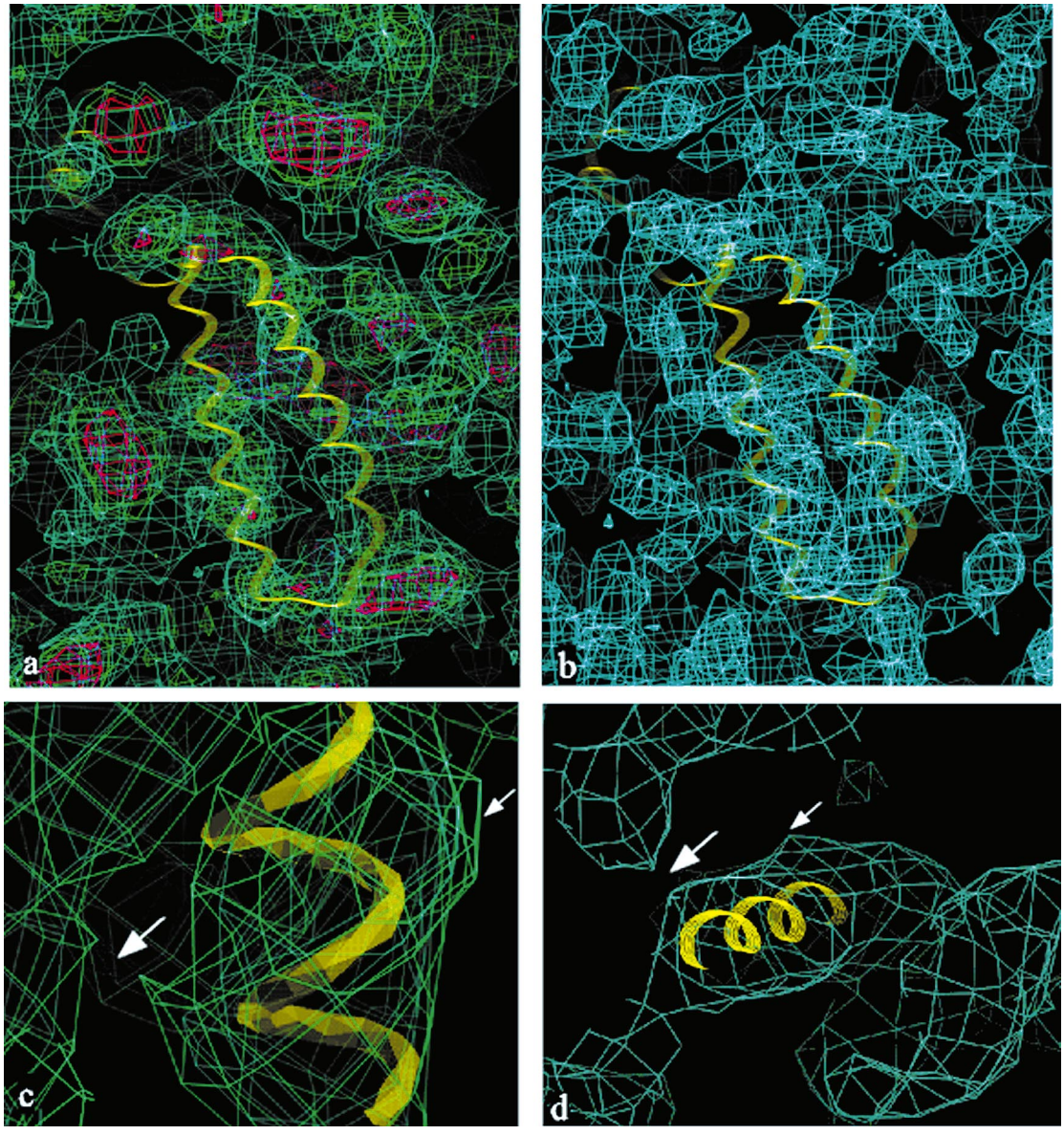

Figure 7
(*a*) Part of the 7.2 Å MIR map of T30S in the expected vicinity of protein S15, contoured at a signal-to-noise signal of 0.7 (green) and 1.1σ (magenta) showing features which resemble the structure of this protein as determined by NMR and X-ray crystallography. Two-thirds of the protein's backbone is overlaid on it. Note the fit of most of the main helices, and the missing density around the flexible chain, except for its helical end. The regions coloured red are of a higher density, presumably hosting RNA chains. (*b*) The area shown in (*a*) of the 5.5 Å extended map, contoured at 0.85σ level. Note that the areas deficient of density in the 7.2 Å map remain so also after the extension to 5.5 Å. (*c*) A view of a typical part of the α-helix. Note the perturbations that may indicate side chains, indicated by white arrows, among which one points at a possible side-chains interaction. (*d*) A cross section through the part of the map shown in (*c*).

motion of this arm despite its flexibility, as frequently happens to long side chains in proteins. The location of the surface of the protein carrying the SH group, TS11, has been determined at the resolution limits of the current MIR map, *i.e.* 7.2 Å. So far, we have used the maleimide reagent, despite its potential chirality, because we could optimize its binding to the ribosome, whereas lower extent of binding was obtained when a non-chiral bridging hand was used.

3.2.2. *Surface ribosomal RNA*. Two-thirds of the mass of bacterial ribosomes are composed of ribosomal RNA. Originally it was assumed that the rRNA provides the scaffold for the ribosome and has a rather passive role in the translation of the genetic information, whereas most of the catalytic activities of the ribosomes are carried out by the ribosomal proteins. During the last decade the participation of rRNA in the functional activities of the ribosome has been clearly demonstrated. These findings stimulated a large volume of studies that showed, among other things, that a large portion of the rRNA is located on the surface of the particles. Experiments aimed at mapping the surface rRNA were initiated over a decade ago (Tapprich & Hill, 1986; Oakes *et al.*, 1986; Ricker & Kaji, 1991). In these procedures synthetic oligodeoxynucleotide probes of 8–20 nucleotides, complementary to specific rRNA sequences, are hybridized to the ribosomal particles and alterations in activity, binding and recognition are monitored (Weller & Hill, 1992). Direct visualization of the hybridization by EM is possible, providing that the cDNA oligomers carry attached markers that can be seen by electron microscopy. For example, biotinylated oligomers that, once hybridized, were reacted with avidin, led to suggestions about the localization of selected rRNA regions (Oakes *et al.*, 1990; Oakes & Lake, 1990). In addition, radioactive photolabile cDNA probes were used for probing specific rRNA regions, in order to highlight their neighbours (Alexander *et al.*, 1994) and to verify inter-components distances determined by other methods.

Complementary DNA oligomers are being exploited by us for the derivatization of ribosomal crystals and for flagging the locations of the rRNA regions targeted by them, taking advantage of heavy atoms that were attached to the DNA oligomers prior to their hybridization. We choose the sequences according to their affinity and specificity, based on previous solution measurements (*e.g.* Weller & Hill, 1992; Oakes *et al.*, 1990; Oakes & Lake, 1990). The length of the oligomers, typically 10–22 nucleotides, is designed to increase the stability of the expected hybrid double-helix. Non-modified oligomers are being diffused into native T30S crystals. Their influence on the internal order of the crystals is used to indicate whether the region with which they were supposed to interact is involved in the crystal network or exposed to the solvent.

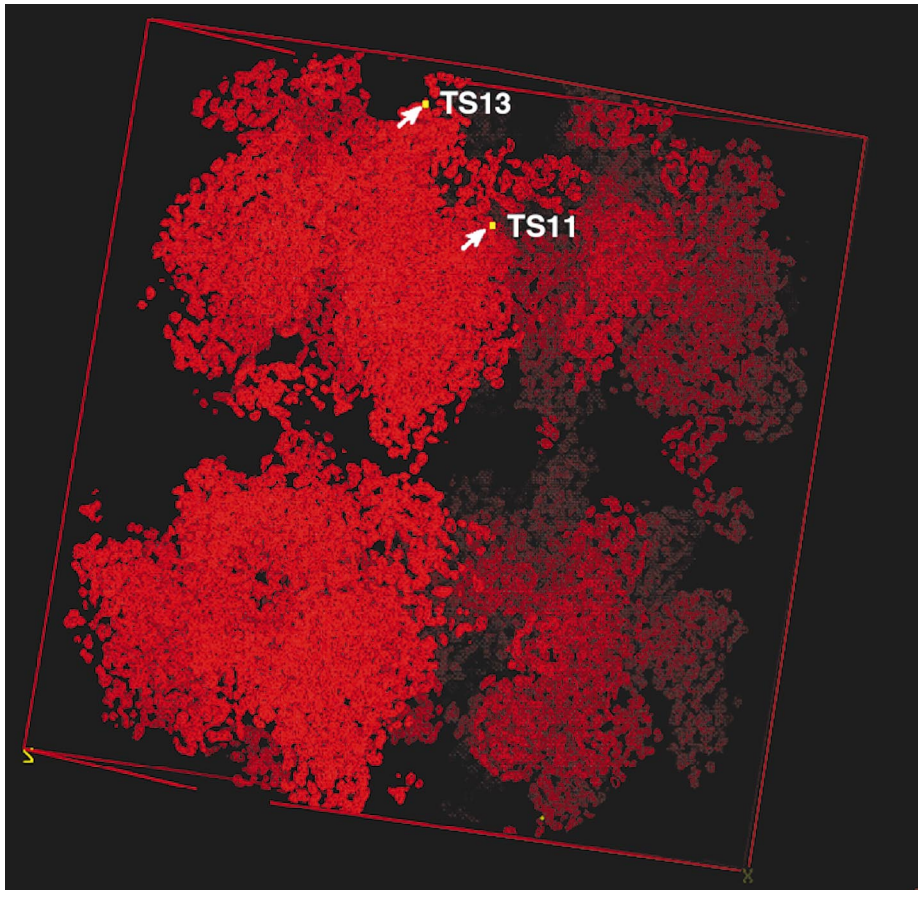

Figure 8
The locations of the tetrairidium clusters in the 7.2 Å MIR map of T30S, shown as yellow squares, with their suggested assignments.

The oligomers that do not cause substantial resolution drop are modified by heavy atoms, either in their cytidines (Dale *et al.*, 1975, Dale & Ward, 1975; Banfalvi & Sarkar, 1995) or terminal phosphates (Alefelder *et al.*, 1998). Alternatively, the heavy atoms are attached to thiolated nucleotides. The degree of hybridization of the modified DNA oligomers is being tested in solution, and those that display a high affinity are being used either for soaking experiments or for hybridization in solution and subsequent co-crystallization.

Over a dozen cDNA oligomers have been checked so far, targeting seven regions. Among them, those matching the 5′ end of the 16S RNA, as well as two regions near helix 41 [nomenclature adopted from that suggested for the 16S RNA from *E. coli*, according to Brimacombe (1995)], did not cause crystal damage, allowing data collection to 3.5–3.9 Å. Those directed to the 3′ end caused a drop of resolution to 6–7 Å, but yielded data with reasonable quality at this limit. These results are in agreement with the level of exposure expected for the 5′ and the 3′ ends of the 16S RNA in the 7.2 Å map, according to our current interpretation. Preliminary crystallographic analysis was performed for the 5′ end hybridized crystals. These led to difference Patterson maps showing peaks which should account for most of the six mercury atoms that were bound to the 21 nucleotides DNA. It is noteworthy that, assuming double-helical conformation, this oligomer should be of over 70 Å in length.

Interestingly, no data could be collected from crystals to which we diffused DNA oligomers complementing the rRNA domain around base 1400, since they introduced a resolution drop to 12–15 Å accompanied by a dramatic increase in the mosaic spread. This '1400 region', also called 'the decoding domain', is the site of the interaction of the small subunit with tRNA, mRNA and other ligands, such as aminoglycoside antibiotics, identified using crosslinking, chemical footprinting, site-directed mutagenesis and protection experiments (O'Connor *et al.*, 1997; Merryman *et al.*, 1999). According to our current interpretation of the 7.2 Å map, the interparticle contacts that form the crystal network exploit many of the regions involved in binding to the large subunit in the associated 70S ribosome, benefiting from the high binding affinities of these regions. Consequently, the decoding domain is extensively involved in crystal-packing contacts, and is therefore not available for smooth and efficient cDNA binding. However, it is conceivable that its high affinity to the complementary oligomer caused its penetration into the crowded area between the two T30S particles. Consequently, partial hybridization may occur despite the steric hindrances, on the expense of the loss of the crystal network.

An additional risk associated with using the heavy-atom -modified DNA oligomers for derivatization stems from their dual chemical nature. Special effort is made to minimize the chemical reactivity of the heavy atoms that are bound to the DNA oligomers in order to avoid their binding to undesired positions. However, mixed proteins/RNA markers may be of high interest in other cases. An example is diaqua-cisplatin that, in addition to its expected interactions with protein moieties in a fashion similar to that found for other platinum compounds, it should interact with specific sequences (*e.g.* GG) on double- and single-strand RNA chains (Reeder *et al.*, 1997). Preliminary results show that among the binding sites of this compound, some were detected in difference maps using other Pt compounds.

4. The large ribosomal subunit

In general the large subunit is more rigid and stable than the small one. Therefore it crystallizes better. Indeed, among 18 crystal types of the 50S particle which were grown by us, three types were found suitable for crystallographic studies at varying detail (Berkovitch-Yellin *et al.*, 1992). Two of them display contradictory properties. Thus, T50S crystals yield quality data but extend only to low resolution, 9–10 Å (Volkmann *et al.*, 1990), whereas those diffracting to 2.7 Å, of H50S (von Böhlen *et al.*, 1991), display undesirable properties, such as high radiation sensitivity with severe deviations from isomorphism, that impose considerable problems in the course of the determination of their structure (Yonath *et al.*, 1998). Consequently, despite the prospects of reaching higher resolution, so far the electron density maps available for H50S extend only to 7–9 Å (Yonath & Franceschi, 1998; Yonath *et al.*, 1998; Ban *et al.*, 1998; Harms *et al.*, 1999; Weinstein *et al.*, 1999). At these resolution ranges the maps are confined to show mainly the overall structure of the particles and their gross structural features, such as the tunnel that spans the large ribosomal subunit. This tunnel, of over 100 Å in length and a diameter of 20–25 Å, was detected in ribosomes from all kingdoms, eubacteria, archea and eukaryotes (Milligan & Unwin, 1986; Yonath *et al.*, 1987, 1998; Stark *et al.*, 1995; Frank *et al.*,. 1995, Verschoor *et al.*, 1998; Dude *et al.*, 1998; Yonath & Franceschi, 1998; Ban *et al.*, 1998).

Some deviations from the cryo-EM reconstructions have been observed in the 10 Å MIRAS map of H50S. The outer borders of the two prominent features of the large ribosomal subunit, the surface proteins HL1 and HL12, are less well defined (Fig. 2). This is presumably because of the limited contrast between the average electron density of proteins (Anderson & Hovmöller, 1998) and that of the solution within the crystals (3 *M* KCl). It is of interest that the map constructed by a combination of SIR and molecular replacements, exploiting unified-density cryo-EM reconstructions, looks more similar to the EM reconstruction used in the MR studies (Ban *et al.*, 1998), presumably because the density of the ribosomal proteins was artificially raised. Indeed, our current 8 Å MIRAS map of H50S shows more detail. Thus, between the elongated dense regions traceable as rRNA located at various directions, patches of lower density, interpretable as r-proteins, are clearly seen.

The MIRAS map of H50S (Fig. 2) provides possible reasoning for the odd combination of the properties of

these crystals: high resolution accompanied by problematic diffraction. These crystals suffer from a low level of isomorphism, substantial radiation sensitivity, observed especially at the higher-resolution ranges, 2.7–5 Å, instability of the longest unit-cell axis and non-isotropic high mosaicity. The high resolution may result from the extensive interparticle contacts concentrated in parts of the unit cell. The very narrow interparticle contact region holding together the longest unit-cell axis (564 Å), which is surrounded by an extremely large solvent region, may explain the low level of isomorphism. This feature may also be the cause for the problematic morphology (extremely thin plates, of a few micrometres thickness), the instability of the *c*-axis and the marked tendency for fragmentation and layer-sliding. It can also explain how large clusters, such as W30 (Table 2; Alizadeh *et al.*, 1985), diffuse readily into and through the H50S crystals and why they may introduce subtle non-isomorphism and lead to limited or less reliable phases.

The packing arrangements of T50S and H50S obtained by SIRAS and MIRAS were confirmed by molecular replacement searches, utilizing the 17 Å cryo-EM reconstruction of T50S. Rotation and translation searches, performed for T50S at 20–40 Å, resulted in a single unique solution exhibiting normal interparticle contacts without overlap. The two major SIRAS sites were placed in the map assembled with the MR phases and found to be in crystallographically sound positions (Yonath & Franceschi, 1998; Harms *et al.*, 1999). Furthermore, the major Ta_6Br_{14} SIRAS site was detected in a difference Fourier map based on the MR phases. For H50S, satisfactory scores were obtained (93% correlation and an *R*-factor of 27% for resolution lower than 60 Å; 39–50% correlation and an *R*-factor 42–47% for the resolution shells between 30 and 95 Å) and the MR phases confirmed the previously determined major site of the strongest H50S derivative, Ta_6Br_{14} (Yonath *et al.*, 1998; Harms *et al.*, 1999; Weinstein *et al.*, 1999). Interestingly, similarities were detected between this packing arrangement and that found for the same crystal type by another group (Ban *et al.*, 1998), although the orientations of the particles appear to differ (Harms *et al.*, 1999).

5. Conclusions and prospectives

The increasing sophistication of the instrumentation at the synchrotron radiation beamlines, the construction of features required for efficient data collection according to the specifications required for work with sensitive systems, and the significant advances in computation power provided the means to add the ribosomes to the list of complexes for which structure determination seems to be feasible. We have shown that low- and medium-resolution MIR and MIRAS maps, exhibiting the external shapes and large internal features, can be constructed for ribosomal particles. Furthermore, significant parts of these maps can be interpreted at a level close to molecular resolution, and selected locations on the ribosomal particles can be revealed by covalently bound medium-size heavy-atom compounds, such as a tetrairidium cluster. As seen, despite the long list of serious crystallographic problems, the way to structure determination has been paved for the small subunit and is progressing for the large one.

For higher-resolution studies, the frequently found low level of isomorphism and the radiation sensitivity of the ribosomal crystals make MAD phasing advantageous. All the heavy-atom compounds used by us may be suitable for this aim as their fluorescence curves fall within the usable synchrotron radiation energies. Among them, Ta_6Br_{14} may be an attractive compound, as it contains two different moieties, each with a significant anomalous signal. However, the MAD experimental requirements are very demanding as the anomalous signals are significantly lower than those obtained per heavy atom with MIR. Hence, quantitative binding is desired and we introduced recombinant methods to facilitate it. We aim at extensive selenation or at heavy-atom modifications *via* inserted sulfhydryl groups, as performed in the nucleosome research (Luger *et al.*, 1997). Since totally reconstituted particles did not yield well diffracting crystals, we focus on proteins that can be quantitatively and reversibly detached by chemical means, mutations or gene knockouts. The same proteins are also suitable for pre-crystallization heavy-atom binding.

As seen above, a wealth of structural information could already be extracted from the MIR map of T30S with expectations for reaching comparable detail from H50S. Of particular interest are several architectural elements, showing high versatility in the modes of interaction between rRNA and r-proteins. In addition, some clues regarding the assembly of the ribosomal particles may be suggested in this preliminary stage. Thus, observing a conformation close to that of the active state in the T30S crystals led to the design of experiments aimed at obtaining higher-quality diffraction by further re-activation of the crystallized particles. Proceeding along these lines, we expect to shed light on the intriguing questions associated with the functional flexibility of the small ribosomal subunit. Since the extension of the phases to near-atomic resolution appears feasible, and since we showed that unbiased positioning is possible, we expect to obtain a fairly detailed structure. Moreover, we plan not only to determine the internal ribosome structure but also to monitor its functional dynamic aspects. For this aim we not only crystallize the small particles at various conformational states, but also co-crystallize the particles with tailor-made ligands, such as antibiotics or complementary DNA to exposed single-strand rRNA regions, or let these materials diffuse into the already formed crystals. Examination of changes in the crystal behaviour upon binding of such ligands indicated the level of their involvement in crystal forces and/or in functional recognition. Binding of metal compounds to these ligands should enable their unbiased positioning, and provide indispensable information required for map interpretation. Suitable examples, like the freezing of the ribo-

somal structure by antibiotic binding, are mentioned above. Others will be anchored on biochemical information now available. An example of structure–function interplay is our attempt to follow the path of nascent protein chains. To shed light on the dynamic driving forces participating in the newly born protein movement, we co-crystallized complexes of H50S with short nascent polypeptides (Berkovitch-Yellin *et al.*, 1992) and plan to attach them to heavy atoms at the amino-acid level.

APPENDIX *A*
Some crystallographic detail

The high-resolution T30S crystals (T30S-HR) were grown as described earlier for the T30S-LR system with a few modifications, associated mainly with milder procedures (Yonath *et al.*, 1988; Harms *et al.*, 1999). Synchrotron radiation data were collected from T30S-HR and its derivatives at F1 (CHESS), ID2 (ESRF), ID19 (APS), BW6 and BW7b (DESY).

Over 22000 reflections were included for the construction of a 7.2 Å MIR of T30S, which was extended partially to 5.5 Å by density modification techniques. Four derivatives were used and their sites were verified by difference Patterson and difference Fourier procedures. FOM (total) = 0.671, phasing power = 1.2–1.4, Rcullis = 0.88–0.91. 60 cycles of density modification were performed (until convergence was achieved), assuming 65% solvent and a Wang radius of 20 Å.

The crystals of T50S and of H50S were grown according to the published procedures (Volkmann *et al.*, 1990; von Böhlen *et al.*, 1991). Those of T50S diffract nominally to 8.7 Å, but yield useful data only to 10 Å. Synchrotron radiation data were collected to 10 Å from native and Ta_6Br_{14}-soaked crystals of T50S at three wavelengths (1.2547, 1.2555 and 1.2600 Å), aiming at obtaining an optimized anomalous signal from the Ta_6Br_{14}-derivatized crystals. Isomorphous and anomalous difference Patterson maps were constructed and two major sites were used for initial SIRAS phasing (Baker *et al.*, 1990). The SIRAS refinement led to: Rcullis = 0.59, 0.87, for total and anomalous, respectively, and phasing power = 1.95 and FOM = 0.58.

Synchrotron radiation data were collected from H50S crystals at all the stations reported in the acknowledgement from over 50 crystals at several resolution ranges between 2.7 and 300 Å. Different wavelengths between 0.78 and 1.26 Å, dictated by the specific synchrotron radiation stations, were used for MIR studies. For collecting anomalous data of Ta_6Br_{14}, the data were collected at 1.2547, 1.2555 and 1.2600 Å.

Various detectors (film, off- and on-line imaging-plate detectors and CCD cameras) were employed. A total of 15 heavy-atom sites of the three derivatives (Ta_6Br_{14}, W12 and W17; Table 2) were included. The positioning of the heavy-atom sites was performed by a combination of difference Patterson and Fourier methods, based on the major position of Ta_6Br_{14}, found to be stable and consistent in all resolution ranges up to 5 Å. Each heavy-atom position was cross-verified and refined by *MLPHARE* with maximum likelihood. Since the contribution of the two W clusters was negligible beyond 10 Å, their scattering curves were approximated by spherical averages of their corresponding radii (W17 = 10 Å and W12 = 8–9 Å). The Ta_6Br_{14}, however, was treated as by Knäblein *et al.* (1997) owing to its potential to the higher-resolution shells. Mean FOM = 0.63, Rcullis = 0.7–0.9, phasing power = 1.25. The map was solvent flattened: one cycle, assuming 54% solvent.

APPENDIX *B*
Abbreviations

70S, 50S, 30S: the whole ribosome and its two subunits from prokaryotes, respectively. A letter prefix to the ribosomal particles or ribosomal proteins represents the bacterial source (*e.g.* E = *Escherichia coli*; T = *Thermus thermophilus*; H = *Haloarcula marismortui*). The names of the ribosomal proteins are composed of a prefix showing the bacterial source, the letters L or S showing that this protein is of the large or small subunit, and a running number according to sequence homology considerations. tRNA and rRNA: transfer and ribosomal RNA; MIR: multiple isomorphous replacement; MIRAS: multiple and single isomorphous replacement combined with anomalous scattering; MAD: multiwavelength anomalous dispersion; MR: molecular replacement. The chemical formula of the tetrairidium cluster (including its reactive bridging arms), as well as TAMM, TIR, Hg_6, W12, W17 and W30 are given in Table 2.

Thanks are given to M. Safro for active participation in phasing, to M. Wilchek for indispensable advice, W. Jahn, W. Preetz and M. Pope for their generous gifts of heavy-atom compounds, M. Eisenstein for predicting the conformational elements of TS11 and TS9, C. Radzwill, H. Burmeister, R. Albrecht, C. Glotz, J. Müssig, C. Paulke, M. Laschever, S. Meier, Y. Halfon and K. Knaack, for their excellent contributions in the different stages of these studies. Data were collected at the EMBL and MPG beamlines at DESY; F1 at CHESS, Cornell University; ID2, ID13, D2AM at ESRF, Grenoble; BL26 at the Photon Factory, KEK, Japan and ID19 at APS, USA. Support was provided by the Max-Planck Society, the US National Institute of Health (NIH GM 34360), the German Ministry for Science and Technology (BMBF 05-641EA) and the Kimmelman Center for Macromolecular Assembly at the Weizmann Institute. AY holds the Martin S. Kimmel Professorial Chair.

References

Alefelder, S., Patel, B. K. & Eckstein, F. (1998). *Nucleic Acids Res.* **26**, 4983–4989.

Alexander, R. W., Muralikrishna, P. & Cooperman, B. S. (1994). *Biochemistry*, **33**, 12109–12118.

Alizadeh, M. H., Harmalker, S. P., Jeannin, Y., Martin-Frere, J. & Pope, M. T. (1985). *J. Am. Chem. Soc.* **107**, 2662–2669.
Anderson, K. M. & Hovmoeller, S. (1988). *Z. Kristallogr.* **213**, 369–373.
Baker, P. J., Farrants, G. W., Stillman, T. L., Britton, K. L., Helliwell, J. R. & Rice, D. W. (1990). *Acta Cryst.* A**46**, 721–725.
Ban, N., Freeborn, B., Nissen, P., Penczek, P., Graussucci, R. A., Sweet, R., Frank, F., Moore, P. & Steitz, T. (1998). *Cell*, **93**, 1105–1115.
Banfalvi, G. & Sarkar, N. (1995). *DNA Cell Biol.* **14**, 445–450.
Berkovitch-Yellin, Z., Bennett, W. S. & Yonath, A. (1992). *CRC Rev. Biochem. Mol. Biol.* **27**, 403–444.
Böhlen, K. von, Makowski, I., Hansen, H. A. S., Bartels, H., Berkovitch-Yellin, Z., Zaytzev-Bashan, A., Meyer, S., Paulke, C., Franceschi, F. & Yonath, A. (1991). *J. Mol. Biol.* **222**, 1–15.
Brimacombe, R. (1995). *Eur. J. Biochem.* **230**, 365–383.
Capel, M. S., Kjeldgaard, M., Engelman, D. M. & Moore, P. B. (1988). *J. Mol. Biol.* **200**, 65–87.
Clemons, W. M., Davies, C., White, S. & Ramakrishnan, V. (1998). *Structure*, **6**, 429–438.
Cusack, S. (1999). *Curr. Opin. Struct. Biol.* **9**, 66–73.
Dale, R., Martin, E., Livingston, D. C. & Ward, D. C. (1975). *Biochemistry*, **14**, 2447–2457.
Dale, R. & Ward, D. C. (1975). *Biochemistry*, **14**, 2458–2469.
Draper, D. E. & Reynoldo, L. P. (1999). *Nucleic Acids Res.* **27**, 381–388.
Dude, P., Wieske, M., Stark, H., Schatz, M., Stahl, J., Zemlin, F., Lutch, G. & van Heel, M. (1998). *Structure*, **6**, 398–399.
Frank, F., Zhu, J., Penczek, P., Li, Y., Srivastava, S., Verschoor, A., Radamacher, M., Grassucci, R., Lata, A. K. & Agrawal, R. K. (1995). *Nature (London)*, **376**, 441–444.
Gabashivili, I. S., Agrawal, R. K., Grassucci, R. & Frank, J. (1999). *J. Mol. Biol.* **286**, 1285–1291.
Harder, K. & Preetz, W. (1990). *Z. Anorg. Chem.* **591**, 32–40.
Harms, J., Tocilj, A., Levin, I., Agmon, I., Koelln, I., Stark, H., van Heel, M., Cuff, M., Schluenzen, F., Bashan, A., Franceschi, F. & Yonath, A. (1999). *Structure.* In the press.
Hosaka, H., Nakagawa, A., Tanaka, I., Harada, N., Sano, K., Kimura, M., Yao, M. & Wakatsuki, S. (1997). *Structure*, **5**, 1199–1208.
Jahn, W. (1989). *Z. Naturforsch. Teil B*, **44**, 79–82.
Kleywegt, G. J. & Jones, T. A. (1997). *Acta Cryst.* D**53**, 179–185.
Knäblein, J., Neuefeind, T., Schneider, F., Bergner, A., Masserschmidt, A., Löwe, J., Steipe, B. & Huber, R. (1997). *J. Mol. Biol.* **270**, 1–7.
Krumbholz, S., Schlünzen, F., Harms, J., Bartels, H., Kölln, I., Knaack, K., Bennett, W. S., Bhanumoorthy, P., Hansen, H. A. S., Volkmann, N., Bashan, A., Levin, I., Tocilj, A. & Yonath, A. (1998). *Period. Biol.* **100**(S2), 119–125.
Lata, A. R., Agrawal, R. K., Penczek, P., Grassucci, R., Zhu, J. & Frank, J. (1996). *J. Mol. Biol.* **262**, 43–52.
Liljas, A. & Al-Karadaghi, S. (1997). *Nature Struct. Biol.* **4**, 767–771.
Luger, K., Maeder, A. W., Richmond, R. K., Segent, D. F. & Richmond, T. J. (1997). *Nature (London)*, **389**, 251–260.
Malhotra, A., Penczek, P., Agrawal, R. K., Gabashivili, I. S., Grassucci, R. A., Junemann, R., Burkhardt, N., Nierhaus, K. H. & Frank, J. (1998). *J. Mol. Biol.* **280**, 103–115.
Merryman, C., Moazed, D., McWhirter, J. & Noller, H. F. (1999). *J. Mol. Biol.* **285**, 97–105.
Milligan, R. & Unwin, P. N. T. (1986). *Nature (London)*, **319**, 693–696.
Moazed, D. & Noller, H. F. (1990). *J. Mol. Biol.* **211**, 135–145.
Mueller, F. & Brimacombe, R. (1997). *J. Mol. Biol.* **271**, 524–544.
Nikonov, S., Nevskaya, N., Eliseukina, I., Fomenkova, N., Nikulin, A., Ossina, N., Garber, M., Jonsson, B.-H., Briand, C., Al-Kadaghi, S., Svensson, A., Æevarsson, A. & Liljas, A. (1996). *EMBO J.* **15**, 1350–1359.
Novotny, V. & Nierhaus, K. H. (1988). *Biochemistry*, **27**, 7051–7055.
Oakes, M. I., Clark, M. W., Henderson, E. & Lake, J. A. (1986). *Proc. Natl Acad. Sci. USA*, **83**, 275–279.
Oakes, M. I. & Lake, J. A. (1990). *J. Mol. Biol.* **211**, 897–906.
Oakes, M. I., Kahan, L. & Lake, J. A. (1990). *J. Mol. Biol.* **211**, 907–918.
O'Connor, M., Thomas, C. L., Zimmermann, R. A. & Dahlberg, A. E. (1997). *Nucleic Acids Res.* **25**, 1185–1193.
Ramakrishnan, V. & White, S. W. (1998). *Trends Biochem. Sci.* **23**, 208–212.
Reeder, F., Guo, Z., Murdoch, P. D., Corazza, A., Hambley, T. W., Berners-Price, S. J., Chottard, J. C. & Sadler, P. J. (1997). *Eur. J. Biochem.* **249**, 370–382.
Richmond, T. J., Finch, J. T., Rushton, B., Rhodes, D. & Klug, A. (1984). *Nature (London)*, **311**, 532–537.
Ricker, R. D. & Kaji, A. (1991). *Nucleic Acid Res.* **19**, 6573–6578.
Sagi, I., Weinrich, V., Levin, I., Glotz, C., Laschever, M., Melamud, M., Franceschi, F., Weinstein, S. & Yonath, A. (1995). *Biophys. J.* **55**, 31–41.
Schluenzen, F., Hansen, H. A. S., Thygesen, J., Bennett, W. S., Volkmann, N., Levin, I., Harms, J., Bartels, H., Bashan, A., Berkovitch-Yellin, Z., Sagi, I., Franceschi, F., Krumbholz, S., Geva, M., Weinstein, S., Agmon, I., Boeddeker, N., Morlang, S., Sharon, R., Dribin, A., Peretz, M., Weinrich, V. & Yonath, A. (1995). *J. Biochem. Cell Biol.* **73**, 739–749.
Stark, H., Mueller, F., Orlova, E. V., Schatz, M., Dube, P., Erdemir, T., Zenin, F., Brimacombe, R. & Van Heel, M. (1995). *Structure*, **3**, 815–821.
Stöffler, G. & Stöffler-Meilicke, M. (1986). *Structure, Function and Genetics of Ribosomes*, edited by B. Hardesty & G. Kramer, pp. 28–46. Heidelberg/NY: Springer Verlag.
Tanaka, I., Nakagawa, A., Hosaka, H., Wakatsuki, S., Mueller, F. & Brimacombe, R. (1998). *RNA*, **4**, 542–550.
Tapprich, W. E. & Hill, W. E. (1986). *Proc. Natl Acad. Sci. USA*, **83**, 556–560.
Trakhanov, S. D., Yusupove, M. M., Shirokov, V. A., Garber, M. B., Mitscher, A., Ruff, M., Tierry, J.-C. & Moras, D. (1989). *J. Mol. Biol.* **209**, 327–334.
Verschoor, A., Warner, J. R., Srivastava, S., Grassucci, R. A. & Frank, J. (1998). *Nucleic Acids Res.* **26**, 655–661.
Volkmann, N., Hottentrager, S., Hansen, H. A. S., Zaytzev-Bashan, A., Sharon, R., Berkovitch-Yellin, Z., Yonath, A. & Wittmann, H. G. (1990). *J. Mol. Biol.* **216**, 239–243.
Wada, T., Yamazaki, T., Kuramitsu, S. & Kyogoku, Y. (1999). *J. Biochem.* **125**, 143–150.
Wei, X., Dickman, M. H. & Pope, M. T. (1998). *J. Am. Chem. Soc.* **120**, 10254–10255.
Weinstein, S., Jahn, W., Glotz, C., Schlünzen, F., Levin, I., Janell, D., Harms, J., Kölln, I., Hansen, H. A. S., Glühmann, M., Bennett, W. S., Bartels, H., Bashan, A., Agmon, I., Kessler, M., Pioletti, M., Avila, H., Anagnostopoulos, K., Peretz, M., Auerbach, T., Franceschi, F. & Yonath, A. (1999). *J. Struct. Biol.* In the press
Weller, J. W. & Hill, W. E. (1992). *Biochemistry*, **31**, 2748–2757.
Wimberly, B. T., White, S. W. & Ramakrishnan, V. (1997). *Structure*, **5**, 1187–1198.
Yonath, A. & Franceschi, F. (1998). *Structure*, **6**, 678–684.
Yonath, A., Glotz, C., Gewitz, H. S., Bartels, K., von Boehlen, K., Makowski, I. & Wittmann, H. G. (1988). *J. Mol. Biol.* **203**, 831–833.
Yonath, A., Harms, J., Hansen, H. A. S., Bashan, A., Peretz, M., Bartels, H., Schluenzen, F., Koelln, I., Bennett, W. S., Levin, I., Krumbholz, S., Tocilj, A., Weinstein, S., Agmon, I., Piolleti, M., Auerbach, T. & Franceschi, F. (1998). *Acta Cryst.* A**54**, 945–955.
Yonath, A., Leonard, K. R. & Wittmann, H. G. (1987). *Science*, **236**, 813–816.
Zamir, A., Miskin, R. & Elson, D. (1971). *J. Mol. Biol.* **60**, 347–364.